Journal of Engineering Science and Technology
Vol. 12, No. 6 (2017) 1580 - 1600

A NUMERICAL STUDY OF WATER PROPAGATION AND BREAKING USING SPH METHOD

COELHO J. G.[1,*], OLIVEIRA T. F.[2], BRASIL JR. A. C. P.[2], MARUZEWSKI P.[3]

[1]Department of Mechanical Engineering, Federal University of Triângulo Mineiro
38064-200, Uberaba, MG, Brazil
[2]Department of Mechanical Engineering, University of Brasília,
79300-000, Brasília, DF, Brazil
[3]EDF CIH FM ED, 73373, Le Bourget du Lac, France
*Corresponding Author: josegustavo@icte.uftm.edu.br

Abstract

A breaking wave is a violent natural event that involves highly complex phenomena, such as large deformation of free surface, turbulence, vortex generation, strong interaction between wave and structures, etc. In this work a wave breaking over an inclined surface is simulated using the Smoothed Particle Hydrodynamics (SPH). SPH is a meshless method that uses a Lagrangian referential to account the forces acting over a fluid particle. The formalism of SPH is based on the idea that the flow can be considered as a set of parts of fluid volume in motion using the concept of particles. This work uses a Weakly Compressible Smoothed Particle Hydrodynamics (WCSPH), where the pressure field is determined by a state equation. The code is validated with several benchmark cases, in which the most relevant parameters for the numerical stability of the analyses are varied. Finally, the model is applied to the simulation of breaking waves in coastal regions, determining shear stresses, important parameter for various applications in engineering, such as erosion.

Keywords: SPH, Free surfaces, Wave propagation, Meshless Method, Fluid mechanics.

1. Introduction

The smoothed particle hydrodynamics (SPH) method is relatively recent; it has been introduced by Lucy in 1977 in the context of Astrophysics modeling [1]. Currently, this method was extended to model a wide range of problems in engineering such as elastic materials [2], explosions [3], fluid mechanics [2, 4], and others.

Nomenclatures

c	Numerical speed of sound, m/s
$\boldsymbol{F}$	Force, N
h	Smoothing length, m
L	Characteristic length, m
m_a	Mass of particle a, kg
P	Pressure, Pa
P_a	Pressure of the particle a, Pa
S_{ij}	Filtered strain rate tensor
u_{ab}	Relative velocity of particles a and b, m/s
$\boldsymbol{u}$	Velocity vector, m/s
$\boldsymbol{U_0}$	Characteristic velocity, m/s
$\mathbf{x}_a$	Position vector of the particle a, m
x_{ab}	Distance between particles a and b, m

Greek Symbols

$\nabla_a W(x_{ab})$	Gradient of the kernel related to particle a and b
$\nabla \cdot \boldsymbol{u}_{ab}$	Divergent of the velocity of the particle a
∇^2	Laplacian operator
∇P_a	Gradient of the pressure of particle a and b
π_{ab}	Artificial viscosity, Pa.s
ρ	Density, kg/m^3
ρ_o	Density at the reference pressure, kg/m^3
τ	Sub-grid Reynolds tensor
υ	Kinematic viscosity, m^2/s
υ_t	Eddy viscosity, m^2/s

The SPH is a Lagrangian meshfree method that uses the idea of particles to model the flow. It integrates the hydrodynamic equations of motion for each particle in the Lagrangian formalism, in which physical quantities are computed for each particle trough an interpolation of the values of the nearest neighboring particles; subsequently the particles move according to these values. The laws of conservation of fluid mechanics, in the differential form are transformed into their forms of particle by integral equations through the use of an interpolation function that provides the estimation of probability density function (kernel) of the field variables at one point. Computationally, data is known only in discrete points (particles), so that the integrals are assessed as sums on the neighbouring particles.

The most attractive characteristic of SPH method is the natural adaptation to very complex or variable flow domain since it requires no discretization mesh (or grid) for the description. Because of this, the SPH could be beneficial compared with conventional approaches (Finite Volume Method and Finite Element Method), typically employed in fluid mechanics simulation, mainly regarding free surface or wave propagation problems. In this context, we highlight a work by Dalrymple et al. [5], Zheng and Duan [6] and Li et al. [7], investigating water waves using the SPH method. It is worth mentioning other papers such as by Gotoh et al. [8] and Violeau and Issa [9] who started the modelling of turbulence in the SPH context.

The present study employs SPH method to simulate the flow of breaking waves onto an inclined surface, representative of typical coastal regions, ultimately looking for the shear stresses at the surface. The challenges to represent wave behavior in costal problems using SPH approach have been explored by some recent works. Barreiro et al. [10] and Altomare et al. [11] among others have explored the potentials of the SPH in complex situations of wave breaking problems, pointing out the difficulty to implement and validate the numerical methods in a framework of complex real problems. Wall-particles modelling (with roughness in the slope), realistic turbulence modelling and computation of surface stresses [12] are recent discussions that have to be explored to obtain good results in the use of SPH in this particular free surface flow. The present paper explores some of those difficulties. It presents not only geometrical shape behaviour of the waves in the breaking conditions. The aim is to obtain realistic results that can be compared to the experimental measurements in some benchmark conditions.

The mathematical model considers the compressible continuity and the incompressible moment equations (XSPH) together with the Smagorinsky sub-grid model to account for turbulence. A calibration of numerical parameters and a careful validation process is conducted in this work. Artificially constructed analytical solutions of Navier-Stokes equations in a square cavity were employed to determine the smoothing length and the regularising parameter of the XSPH, for shear driven flows. After that, simulations of propagating and breaking waves were conducted in order to verify the ability of the model in to describe inertial free surface motions. The ParaView platform was used for post-process the simulations data. The work is organized in five sections: the introduction in section 1, the flow mathematical model in given in section 2, followed by a complete description of the XSPH numerical methods in section 3. Section 4 gives all results of the work, including the calibration and validation procedures. Finally, the main conclusions of the work were drawn in section 5.

2. Weakly Compressible Smoothed Particle Hydrodynamics

Our study uses the weakly compressible SPH. In this section the fundamental principles and formulations of the WCSPH model are indicated.

Governing equations

The governing equations of Fluid Mechanics are the continuity and momentum equations, classically expressed for Newtonian Fluid in the differential form by

$$\frac{D\rho}{Dt} = -\rho\nabla\cdot\boldsymbol{u}, \tag{1}$$

$$\frac{D\boldsymbol{u}}{Dt} = -\frac{1}{\rho}\nabla \mathrm{P} + \upsilon\nabla^2\boldsymbol{u} + \boldsymbol{F}, \tag{2}$$

where the material derivative is given by $\frac{D(\ )}{Dt} = \frac{\partial(\ )}{\partial t} + \boldsymbol{u}.\nabla(\ )$. Equations (1) and (2) express the principles of conservations of mass and momentum as experienced by an observer who moves with a fluid material particle. The practice

of SPH simulations, even in the case of small Mach numbers flows, involves the adoption of a compressible formulation [3, 13, 14]. This is justified by the advantages of keeping an explicit numerical scheme, compatible with the Lagrangian approach, and more suitable to a meshless description of the domain. Therefore, a constitutive equation for pressure should be used. For a near incompressible flow, Batchelor [15] suggests a relation like

$$P = \frac{\rho_0 c^2}{\gamma}\left[\left(\frac{\rho}{\rho_0}\right)^{\gamma} - 1,\right] \tag{3}$$

This state equation has proved valid for small variations of pressure and could be used for SPH simulations of liquids, according to Monaghan [13]. This approach depends on the numerical speed of sound, *c*. The practice of SPH simulations have the value of the sound speed, *c*, usually set to allow small variations of density ρ, so that the pressure field could be calculated by the state equation (3). Nevertheless, the choice for the value of c should also ensure that the density does not vary more than 1% [14], in order to keep the validity of the incompressibility hypothesis. One way to estimate an initial value for *c* is by using some scaling arguments [3], so that

$$c^2 \approx \left(\frac{\|\boldsymbol{U}_0\|}{\delta_*}, \frac{\upsilon\|\boldsymbol{U}_0\|}{L\delta_*}, \frac{\|\boldsymbol{F}\|L}{\delta_*}\right), \tag{4}$$

It is worth noting that this is just an initial estimate, and the actual value of *c* must be carefully determined in each simulation.

3. Smoothed Particle Hydrodynamics Formulations

3.1. Core of smoothed particle hydrodynamics

In the formulation of the SPH, the fluid is represented by a discrete set of points, or particles. Every particle has physical properties, such as mass, volume, pressure, velocity and density. All properties vary during evolution, except the mass of the particle, due to the incompressibility hypothesis. These properties represent a spatial average centered on the point of the domain, occupied by the particle. The value of a generic property *A* (scalar, vectorial or tensorial), for a particle at the position $\boldsymbol{x}$, is given by

$$A(\boldsymbol{x}) = \int_{\Omega} A(\boldsymbol{x}')W(\boldsymbol{x} - \boldsymbol{x}')d\boldsymbol{x}', \tag{5}$$

where Ω represents the whole flow domain and W ($\boldsymbol{x}$ –$\boldsymbol{x}'$) is a *kernel* or *interpolation* function and has properties compatible with classical probability density functions. Usually, the kernel is chosen as a compact function where the average process is restricted to a part of the domain defining a certain neighbourhood of the particle. In this study, we use as function a cubic spline defined by Izza 16].

$$W(s) = \frac{10}{7\pi}\begin{cases} 1 - \frac{3}{2}s^2 + \frac{3}{4}s^3 & \text{if } 0 \leq s < 1; \\ \frac{1}{4}(2-s)^3 & \text{if } 1 \leq s < 2; \\ 0 & \text{if } s \geq 2; \end{cases} \quad (6)$$

where $s = x/h$, h is the length of the filter and $x = |\,|(\mathbf{x} - \mathbf{x}')\,|\,|$.

Considering the discrete character of the domain, the integral in Eq. (5) is approximated by a summation over all neighboring particles. So, at the position x of the particle a, the approximation can be rewritten as

$$A(\boldsymbol{x_a}) \approx \sum_b \frac{m_b}{\rho_b} A_b W(x_{ab}), \quad (7)$$

where the index b indicates a sum over all of the neighboring particles in the radius of the particle influence a, m is the mass and x_{ab} is distance between particles a and b.

The smoothing process defined by Eqs. (5) and (6) defines a spatial centered average with radius h, which is associated with a numerical (or artificial) diffusion process. So, if we increase the smoothing length we are also increasing the artificial diffusion and, therefore, we can cause an overstated smoothing of the velocity or pressure gradients. In contrast, if the smoothing length is too small, a well-defined spatial average could not be calculated, because only a few particles would considered by the averaging process [3]. For these reasons, the definition of the smoothing length h is a sensitive task, which must be carried out carefully.

There are different ways to determine the gradient and divergence operators in the SPH method. This study uses the formulation proposed by [3], where the pressure gradient and velocity divergence can be written as

$$\nabla P_a \approx \rho_a \sum_b m_b \left(\frac{P_b}{\rho_b^2} + \frac{P_a}{\rho_a^2}\right) \nabla_a W(x_{ab}), \quad (8)$$

$$\nabla \cdot \boldsymbol{u}_a \approx -\frac{1}{\rho_a} \sum_b m_b \boldsymbol{u}_{ab} \cdot \nabla_a W(x_{ab}). \quad (9)$$

Thus, we represent the Navier-Stokes equations in SPH formalism as

$$\frac{D\rho_a}{Dt} = \sum_b m_b \boldsymbol{u}_{ab} \cdot \nabla_a W(x_{ab}). \quad (10)$$

$$\frac{D\boldsymbol{u}}{Dt} = -\sum_b m_b \left(\frac{P_a}{\rho_a^2} + \frac{P_b}{\rho_b^2} + \Pi_{ab}\right) \nabla_a W(x_{ab}) + \upsilon \nabla^2 \boldsymbol{u}_a + \boldsymbol{F}_a. \quad (11)$$

The term π_{ab} was firstly proposed by Monaghan to improve the stability of the simulation [17]. In this work, this term is modelled as

$$\Pi_{ab} = \begin{cases} \frac{-\alpha \overline{c_{ab}}\, \phi_{ab}}{\overline{\rho_{ab}}} & \text{if } \boldsymbol{u}_{ab} \cdot \boldsymbol{x}_{ab} < 0 \\ 0 & \text{if } \boldsymbol{u}_{ab} \cdot \boldsymbol{x}_{ab} \geq 0, \end{cases} \quad (12)$$

where α is 0.03. The term $\emptyset_{ab} = \frac{h_{ab}\boldsymbol{u}_{ab}.\boldsymbol{x}_{ab}}{|x_{zb}|^2+\varphi^2}$, $\bar{c}_{ab} = \frac{1}{2}(c_a + c_b)$, $\bar{\rho}_{ab} = \frac{1}{2}(\rho_a + \rho_b)$, $h_{ab} = \frac{1}{2}(h_a + h_b)$ and $\varphi = 0.1h$ inserted to avoid dividing it by zero. A further description of the artificial viscosity is found in [3] and [17].

The Newtonian viscous term is determined by different formulation [14, 16]. We use the formulation proposed by [17] given by

$$\upsilon\nabla^2\boldsymbol{u}_a = \boldsymbol{8}\frac{\upsilon_a + \upsilon_b}{\rho_a + \rho_b}\frac{\boldsymbol{u}_{ab}\cdot\boldsymbol{x}_{ab}}{x_{ab}^2 + 0.01h^2}\nabla_a W(x_{ab}), \tag{13}$$

Further details can be found in [3, 18]. As aforementioned, the SPH uses a spatial filter, a feature that resembles the Large Eddy Simulation (LES); therefore, we use a LES approach. In the context of SPH, when moment equation is filtered, we obtain a similar equation, adding the sub-grid Reynolds tensor term. This equation is given by Violeau and Issa [9]

$$\frac{D\bar{\boldsymbol{u}}}{Dt} = -\frac{1}{\rho}\nabla\bar{\mathrm{P}} + \upsilon\nabla^2\bar{\boldsymbol{u}} + \boldsymbol{F} + \frac{1}{\rho}\nabla\cdot\tau, \tag{14}$$

Each component of this tensor is defined as $\tau_{ij} = \rho\left(\bar{u}_i\bar{u}_j - \overline{u_i u_j}\right)$ [8]. Since we deal here with nearly incompressible flows, we assume that $\bar{\rho}_a \approx \rho_a$. Using the Boussinesq hypothesis,

$$\frac{\tau_{ij}}{\rho} = \left(2\upsilon_t\bar{S}_{ij} - \frac{2}{3}k\delta_{ij}\right). \tag{15}$$

The filtered strain rate tensor, $\bar{S}_{ij}$, is determined by

$$\bar{S}_{ij} = -\frac{1}{2}\left(\frac{\partial\bar{u}_i}{\partial x_j} + \frac{\partial\bar{u}_j}{\partial x_i}\right) \tag{16}$$

We have applied the Smagorinsky constitutive model to eddy viscosity, so that$\upsilon_t = (C_s\Delta)^2|\bar{S}|$ where C_s = 0.12 is the Smagorinsky constant [9], Δ is the length scale which is equal to the mean distance between the particles [5]. The norm of the local strain rate tensor is given by $\overline{|S|} = \left(2\bar{S}_{ij}\bar{S}_{ij}\right)^{0.5}$. Thus, the sub-grid Reynolds tensor in relation to the particle a is determined by Gotoh et al. [8]

$$\left(\frac{1}{\rho}\nabla\cdot\tau\right)_a = \sum_{b=1}^{N} m_b\left(\frac{\tau_a}{\rho_a^2} + \frac{\tau_b}{\rho_b^2}\right)\cdot\nabla_a W_{ab}. \tag{17}$$

For the time integration several time step criteria must be satisfied,

$$\Delta t = min\left\{0.25\frac{h}{c}; 0.25\min_a\sqrt{\frac{h}{f_a}}; 0.125\min_x\frac{h^2}{\upsilon}; \iota\frac{h_p}{u_p}\right\}, \tag{18}$$

where ι = 0.005. All these conditions must be satisfied simultaneously. In cases where there is a moving boundary, the latter condition in Eq. (18) is the most restrictive.

Finally, to prevent particle penetration and regularize the velocity field, the velocity equation is rewritten as [19]

$$\frac{D\boldsymbol{x}_a}{Dt} = \boldsymbol{u}_a - \epsilon \sum_{b=1}^{N} \frac{m_b}{\rho_b} \boldsymbol{u}_{ab} W_{ab}, \tag{19}$$

where the constant ε ranges from 0 to 0.5.

This method is a "correction" to the particle velocity proposed by Monaghan [13], and became known as XSPH. This velocity is recalculated considering the velocity of the particle and the average velocity of all the particles interacting with the particle a. Because one chooses a function W with compact support, only the neighboring particles are included in the calculation [3].

The SPH is a dissipative method and the parameter ε is directly connected to this fact. If this parameter is high, numerical dissipation is accentuated. In contrast, if it is small, instabilities are perceived. During this work, we noticed that for problems with confined fluid the best option is $\varepsilon = 0.3$, but, when there is a condition of free surface, we recommend $\varepsilon = 0.03$.

3.2. Boundary conditions

The application of the boundary conditions has been the subject of various developments in recent years. The most popular method uses the idea of the repulsive force, exerted by the wall particles. Thus, the wall particles exert a repulsive force in the fluid particles that are within its radius of influence. This force is given by Monaghan [18]

$$FP_{ab} = \begin{cases} D\left[\left(\frac{r_0}{x_{ab}}\right)^{12} - \left(\frac{r_0}{x_{ab}}\right)^{4}\right]\frac{x_{ab}}{r_{ab}^2} & \text{if} \quad \frac{r_0}{x_{ab}} \leq 1; \\ 0 & \text{if} \quad \frac{r_0}{x_{ab}} > 1. \end{cases} \tag{20}$$

The constant D is the square of the magnitude largest flow velocity. The distance r_0 is approximately equal to the initial distance between the particles. Both, D and r_0 play a key role for the stability of the method.

4. Results

4.1. Analytical solutions

The SPH code is applied on the Stokes' flow and the results are compared to an analytical solution. This analytical solution is described in [20]. A two-dimensional problem in the square domain with unit length is considered. The problem consists in determining the velocity field, $v = (v_x; v_y)$ by

$$\begin{aligned} \boldsymbol{F} &= -\upsilon\nabla^2\boldsymbol{v} + \nabla \mathrm{P}, \\ \nabla \cdot \boldsymbol{v} &= 0 \end{aligned} \tag{21}$$

An analytical solution for equation (21) is obtained by choosing a velocity field $v = (v_1,v_2)$ respecting the continuity equation. We choose a polynomial form of v_1 and v_2 given by

$$v_1 = x_1^2(1-x_1)^2(2x_2 - 6x_2^2 + 4x_2^3), \qquad (22)$$
$$v_2 = -x_2^2(1-x_2)^2(2x_1 - 6x_1^2 + 4x_1^3).$$

It can be observed that the velocity field given by Eq. (22) keeps the non-slip condition over the edges of the square domain. The pressure is set to a constant value throughout the flow field. The velocity field is replaced into Eq. (21) and the body force **F** = (F_1, F_2) is then determined, resulting in

$$\begin{aligned} F_1 &= (-24x_2 + 12)x_1^4 + (48x_2 - 24)x_1^3 + (-48x_2^3 + 72x_2^2 - 48x_2 + 12)x_1^2 + \\ &\quad (48x_2^3 - 72x_2^2 + 24x_2 - 2)x_1 + (1 - 4x_2 + 12x_2^2 - 8x_2^3) \\ F_2 &= \left(48x_2^2 - 48x_2 + 8\right)x_1^3 + \left(-72x_2^2 + 72x_2 - 12\right)x_1^2 + (24x_2^4 \\ &\quad -48x_2^3 + 48x_2^2 - 24x_2 + 4)x_1 + (-12x_2^2 + 12x_2^3 - 12x_2^4) \end{aligned} \qquad (23)$$

The velocity field given by Eq. (22), the body force given by (23) and a constant pressure field are an analytic solution of the Stokes equation in the square domain [0,1] **X** [0,1]. We programmed the body force in the moment equation in order to obey the expressions (23). We expect to recover a velocity field equal to that given by (22). We use the maximum flow velocity, 0,013 m/s, to determine the Reynolds number of simulation, equal to 5×10^{-6}. Another parameter determined by the maximum velocity is the numerical speed of sound, c = 0.13 m/s.

For a first analysis, the amount of particles is estimated using a spatial resolution of the discretization, $a/40$, where a is the length of domain. Thus, the number of fluid particles is 1600. For the post-processing we use the Paraview-Meshless Software, which is free software designed for the analysis of flow with particles.

The boundary conditions are satisfied using the proposed method. For comparison with the analytical result, we created a vertical line in the center of the domain and we determined the horizontal velocity in this line. To determine the error we use the mean square deviation, defined as

$$e = \frac{1}{N}\sum_{i=1}^{N}(s-r)^2, \qquad (24)$$

where s is the numerical result, r the analytical results and n is the amount of particles. The mean square found is 3.43×10^{-3} and the maximum deviation is 6.30×10^{-2}.

To analyse the SPH solutions, we changed some parameters. The first analysis is related to the benefits of using or not the modifications proposed in the XSPH. It can be seen in Fig. 1, that without this correction there are instabilities in the velocity field. Different values were used for the parameter ε, as illustrated in Fig. 1. It was observed that if $\varepsilon \approx 0$, we find instability. In this situation, $\varepsilon = 0.3$ is suggested [3]. If the value of ε is gradually increased, the flow is proportionally more diffusive.

The smoothing length h was also analysed. This parameter is found in relation to the initial particles distance, Δx. The simulations are performed for different $h/\Delta x$ = 1.1, 1.2, 1.3, 1.6, 1.7, 2. 0.

The deviation for different h are indicated in Tables 1 and 2. Figure 2 illustrates the flow in x axis with smoothing lengths $h = \Delta x$ and $h = 1.3\Delta x$. It can be observed that with $h = 1.3\Delta x$ the results are better. This is because the filter with $h = \Delta x$ is small to capture the expected physical effects.

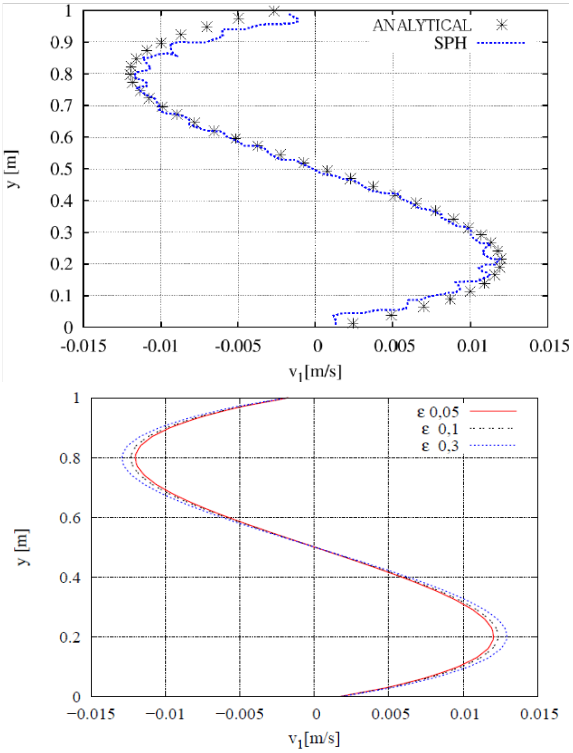

Fig. 1. Horizontal velocity in the vertical center line without XSPH (up) and with different ε (down).

Table 1. Mean square as a function of the smoothing length for 1600 particles.

$h/\Delta x$	e	Maximum deviation
1.1	3.13×10^{-3}	6.30×10^{-2}
1.2	3.40×10^{-4}	5.67×10^{-2}
1.3	3.8×10^{-5}	1.04×10^{-2}
1.6	4.47×10^{-4}	$1.15\times10^{-2.}$
1.7	4.93×10^{-4}	3.02×10^{-2}
2.0	4.15×10^{-3}	5.81×10^{-2}

Table 2. Maximum deviation of the h for 900 particles.

$h\times\Delta x$	e	Maximum deviation
1.2	4.50×10^{-3}	1.57×10^{-2}
1.3	1.10×10^{-3}	1.44×10^{-2}
1.6	6.10×10^{-3}	2.24×10^{-2}
2.0	1.05×10^{-2}	$2.50\times10^{-2.}$

Another parameter analysed was the spatial resolution of discretization. Thus, we ran simulations with 400, 900, 1600, 2500 and 3600 particles. For 400

particles we could not obtain stable simulations. For 900 particles different values were tested for the smoothing length, and the optimum smoothing length is $h = 1.3\Delta x$ (Fig. 2). The simulation with 2500 fluid particles had better results when $h = 1.4\Delta x$. As expected, there was an increase in computational time and a decrease of the deviation when 3600 fluid particles were used. In this case the optimal smoothing length is $h = 1.3\Delta x$.

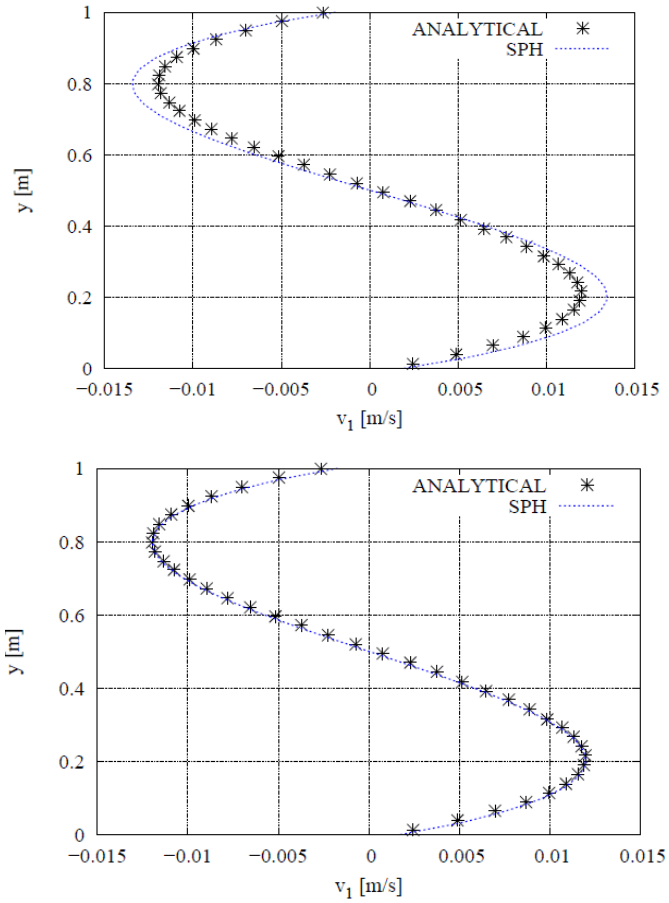

Fig. 2. Horizontal velocity on vertical central line with $h = \Delta x$ (up) and $h = 1.3\Delta x$ (down).

Analysing the results of the simulations with 900, 1600, 2500 and 3600 particles, it can be observed that the optimal value for the smoothing length is around $1.3\Delta n$. Using this value; approximately 21 particles determine the spatial average.

Finally, the model is used to determine the shear stress on an inclined line. This line is formed by the coordinates $(x, y) = (½, 0)$ and $(1,½)$. Figure 3 illustrates a comparison of the analytical and SPH solutions, for discretizations with 900, 1600, 2500, 3600 fluid particles. The analysis of the deviation is indicated in the same figure. It can be seen that when the number of particles is sufficient to accurately calculate parameters such as average velocity, it is also accurate to determine the shear stress.

4.2. Dam break

Another problem studied is the dam break. This example is frequently used to validate numerical methods, particularly with the free surface condition. Figure 4 there is an illustration of the domain, where a = 1 m. The active force on this problem is gravitational and the dam break is performed at time t = 0 s, when the dam is removed. This simulation requires a better spatial resolution of the discretization; therefore, in this case, we use the discretization of $H/50$ that results in 20000 fluid particles. For the wall, we use 4 layers of particles. The smoothing length is $1.3\Delta x$.

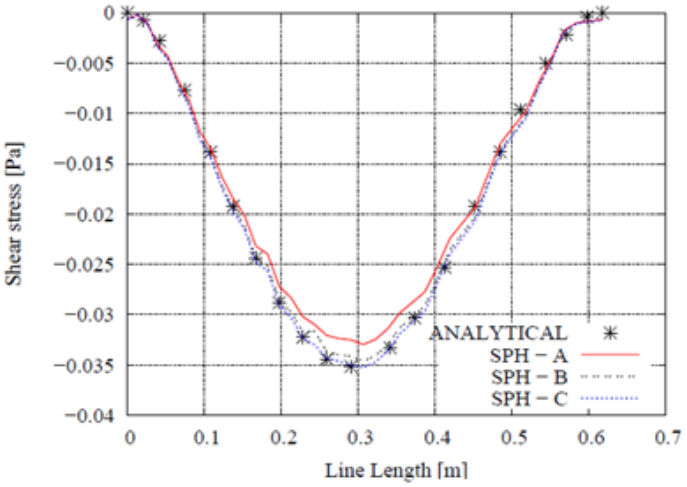

particles	e	maximum deviation
900	4.50×10^{-2}	1.57×10^{-1}
1600	3.10×10^{-3}	1.44×10^{-1}
2500	1.10×10^{-3}	4.24×10^{-2}
3600	2.05×10^{-4}	2.15×10^{-2}

Fig. 3. Comparison of analytical and numerical values of shear stress, where SPH-A has 900 particles; SPH-B has 2500 particles and SPH-C has 3600 particles (up) and mean square and maximum deviation in the calculation of shear stress (down).

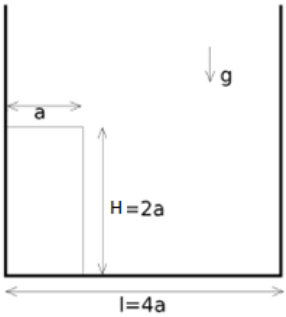

Fig. 4. Geometry of the dam break.

Using negative gravity in direction *y*, Monaghan [18] suggests that the initial density is determined by

$$\rho = \rho_0 \left(1 + \frac{7\rho_0 g(H-y)}{\rho_0 c^2}\right)^{1/7} \tag{25}$$

where ρ_0 = 1000 kg/m^{3}and H is the height of the water in meters. When a dam of height H collapses, an approximate upper bound to the speed u of the water is given by $\boldsymbol{u}_2 = 2gH$ [18]. So, $c = \sqrt{200gH} \approx 63$ m/s, but this value results in a variation of density greater than 1%. For a variation of density under this limit, we adopted c = 100 m/s.

Initially, we tested the value of ε = 0.3, however, it pointed that the displacement fluid is underestimated. To solve this problem, we adopted the value of ε = 0.03, also used by Zheng and Duan [6]. A comparison of this result is illustrated in Fig. 5. It is believed that this variation of the parameter ε is required due to the characteristic problem, where it was previously a confined fluid, and later we have the free surface characteristic. Another comparison established with [21], Fig. 5, with the variation of the displacement of the fluid in relation to time

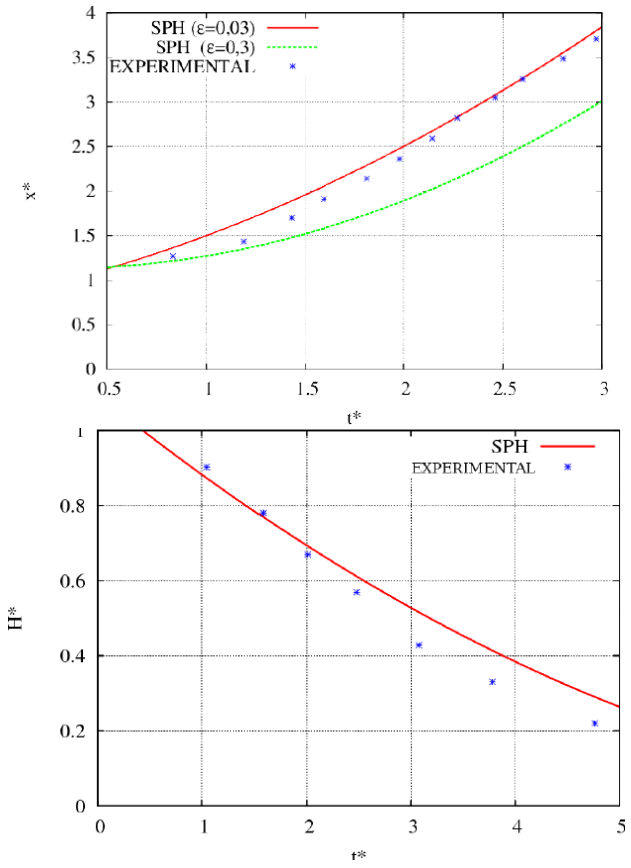

Fig. 5. Comparison with experimental simulation (Koshizuka and Oka [21]) where $X^* = x/a$ and $t^* = t\sqrt{(2g/a)}$ (up) and $H^* = H/(2a)$ e $t^* = t\sqrt{(2g/a)}$ where $\epsilon = 0.03$ (down).

Figure 6 illustrates a comparison of the flow pattern obtained using numerical and experimental [22] results, with the formation of a tube, which is a difficult feature to simulate using conventional numerical methods. The results are satisfactory, revealing the SPH robustness.

4.3. Irregular wave propagation

To validate the SPH model, we included two cases where the flow is governed by field forces and contact forces. The first case simulates the propagation of irregular wave. The domain used is illustrated in Fig. 7. The left wall is responsible for generating irregular waves. To move the wall, we used a signal found in [23], who conducted an experimental study on this sample.

The smoothing length used is $h = 1.3\Delta x$ for all of the particles, except the moving boundary for which we use $h = 0.3\Delta x$ to prevent numerical instabilities. As it is a great domain, we use a spatial resolution of discretization H/40, where H is the water height. This results in 43236 particles (4000 fluid and 3236 wall).The numerical speed of sound is 35.7 m/s and $\varepsilon = 0.03$.

To reproduce the moving boundary, the position and velocity of the particles are externally imposed. Changes in the velocity value may generate high accelerations of the fluid particles causing instabilities. To prevent a high acceleration, we use the smoothing function proposed by Gesteira et al. [24]. Thus, if the wavemaker moves with amplitude A_i and frequency f_i in the interval $t \in [t_{i+1}, t_{i+2}]$ and amplitude A_{i+1}andfrequency f_{i+1} in the interval $t \in [t_i; t_{i+1}]$ then for any t between $(t_i + t_{i+1})/2$ and $(t_{i+1} + t_{1+2})/2$, the oscillatory movement of the movemaker in the direction x is determined by the functions

$$\begin{aligned} x_p(t) &= s_1(t)A_i \sin\big(f_i(t-t_i)\big) + s_2(t)A_{i+1}\sin(f_{i+1}(t-t_{i+1})) \\ u_p(t) &= s_1(t)A_i f_i \cos\big(f_i(t-t_i)\big) + s_2(t)A_{i+1}f_{i+1}\cos(f_{i+1}(t-t_{i+1})) \end{aligned} \quad (26)$$

where $s_1(t) = 0.5(-\tanh((t - t_i)k) + 1)$, $s_2(t) = 0.5(\tanh((t - t_i)k) + 1)$ are smoothing functions and $k = max(f_i; f_{t+1})$.

Figure 8 illustrates the displacement of the wavemaker and the velocity. It is observed that no discontinuity in the velocity is found in the transition between the different cycles.

The results are compared with experimental data found in [23], where Fig. 9 illustrates the elevation at 7, 9 and 10 m from the origin, respectively. As pointed through the comparison, the results are satisfactory at all of the measured points. It can be observed that the difference in amplitude is greater as it moves further from the origin; which occurs because the SPH is a dissipative method. This dissipative process had also been reported by [6].

4.4. Impact of waves

This section will show the impact of waves on an inclined surface. After several trials, we defined the parameters considered ideal for the present case, with a velocity sound of 20, and a smoothing length of h=1.3Δx. The spatial resolution of the discretization was H/100, which is sufficient to capture the desired effects, such as plunging breaking, tube formation, etc. This discretization results in the

number of 40039 particles (39950 fluid and 8089 wall particles). The domain used is analogous to Fig. 4, but with left vertical wall with angulation of 15°. The horizontal length is 0.5 m and the height of the water column is 0.4 m. The horizontal length was chosen to prevent the smoothing of the wave amplitudes indicate in previous examples and, of course, to reduce computational cost. The topic 4.3 to variation of the flow is given by a wavemaker. The displacement of the wavemaker is illustrated in Fig. 10 (a).

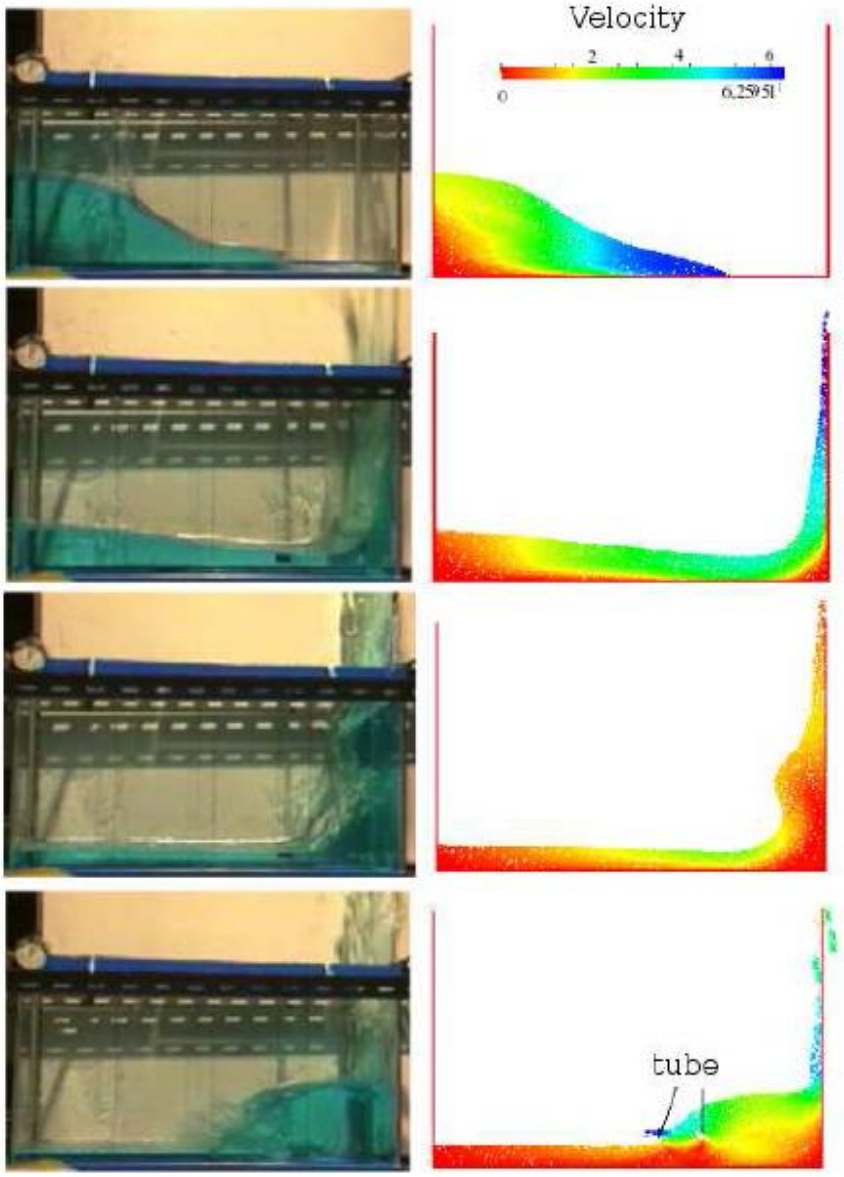

Fig. 6. Comparison of numerical and experimental results, in the 2, 4, 6 and 8 s [22].

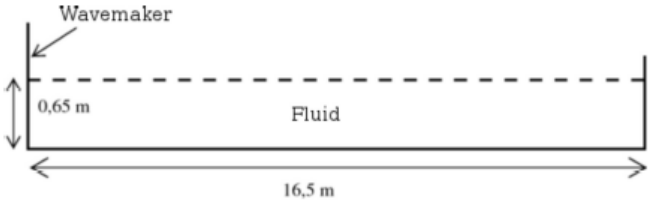

Fig. 7. Initial configuration of the fluid and particles of the wall to reproduce the irregular waves.

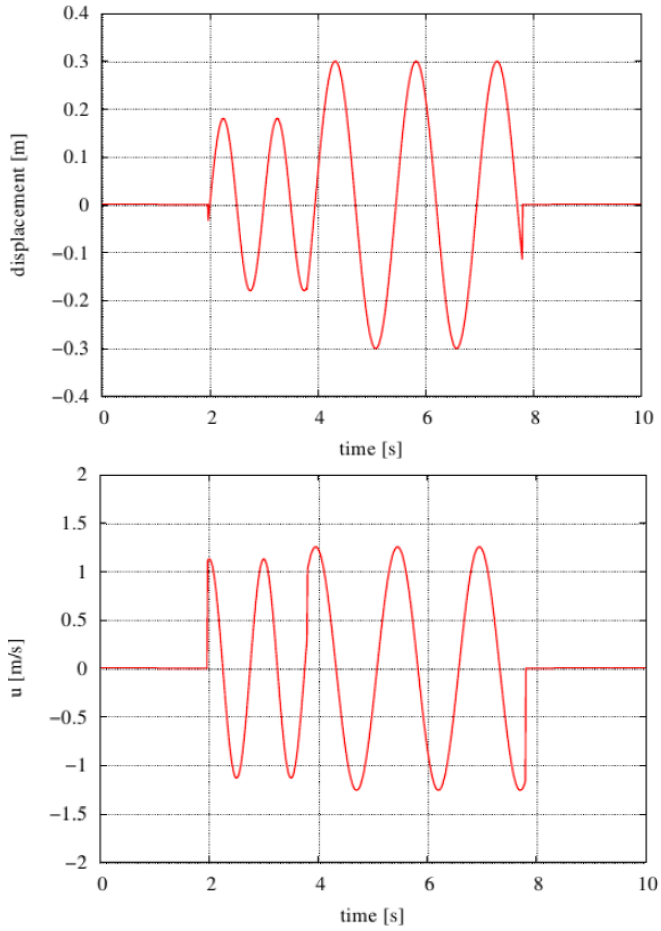

Fig. 8. Displacement (up) and velocity (down) of the wavemaker in the horizontal axis.

Since there are no available experimental data for shear stress distribution along the inclined surface, we established a comparison of the results with the numerical model. According to Xiao and Huang [25], these shear stresses can be computed by Eq. (27). Thus, using the calculated velocity and Eq. (27), we calculated the shear stress and compared the result with the SPH code.

$$\tau(t) = 0.125\rho|u|u, \tag{27}$$

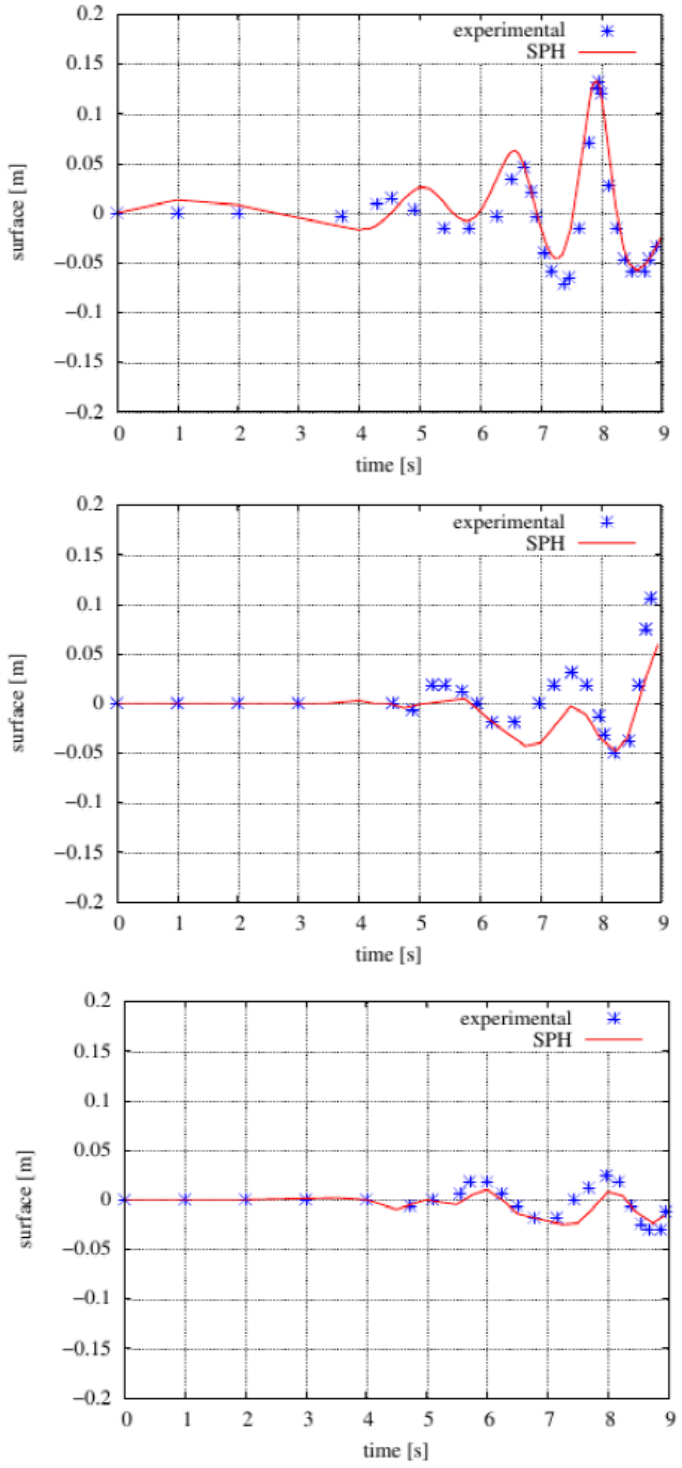

Fig. 9. Elevation of surface at 7, 9 and 10 m of the origin.

To calculate the stresses with the SPH code, we used the ParaView-MeshLess plugin since it offers a number of useful classes that can be used to process meshless date. Fig. 10 illustrates the comparison of the shear stress obtained through the SPH in the inclined surface and the formulation by [25]. As indicated, the SPH produces satisfactory results; it is believed that with better discretization and implementation of wall laws, this result can be improved.

Figures 11 and 12 illustrate the flow and the shear stress in the black line. The shear stress has its greatest value at the time of wave impact, as pointed in these figures. Depending on the direction of the flow, we can observe that the shear stress rapidly changes from positive to negative (or inverse), as Fig.11 for example. The software is capable of determining the rapid flow variation; this is a very important phenomenon for several engineering phenomena, such as the determination of erosion. Now we are able to calculate the shear stress, but the soil data analysis to find the strength is supports is still missing; therefore, further possibilities can lead us to a detailed analysis of the erosion phenomenon.

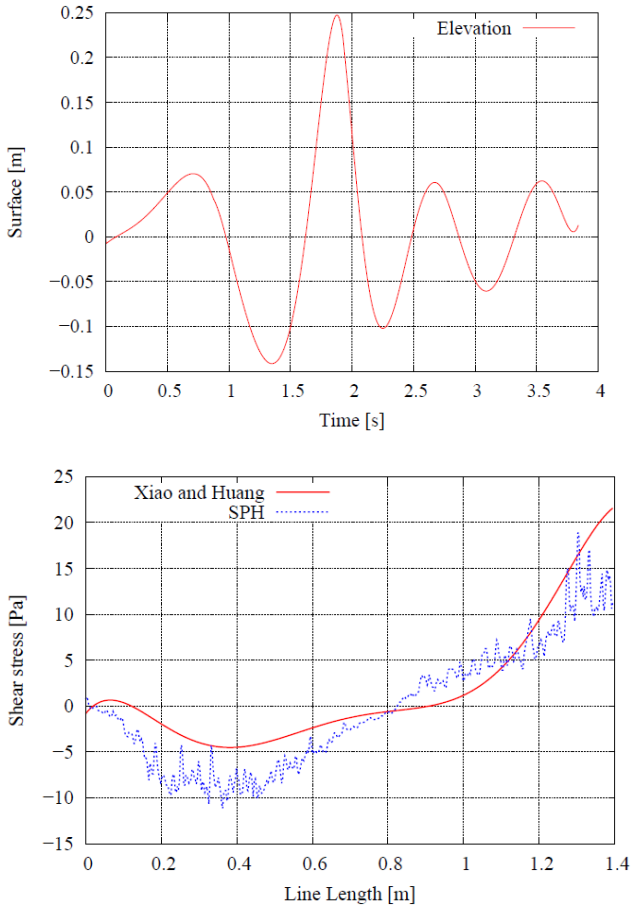

Fig. 10. Profile wave generator and comparison of shear stress.

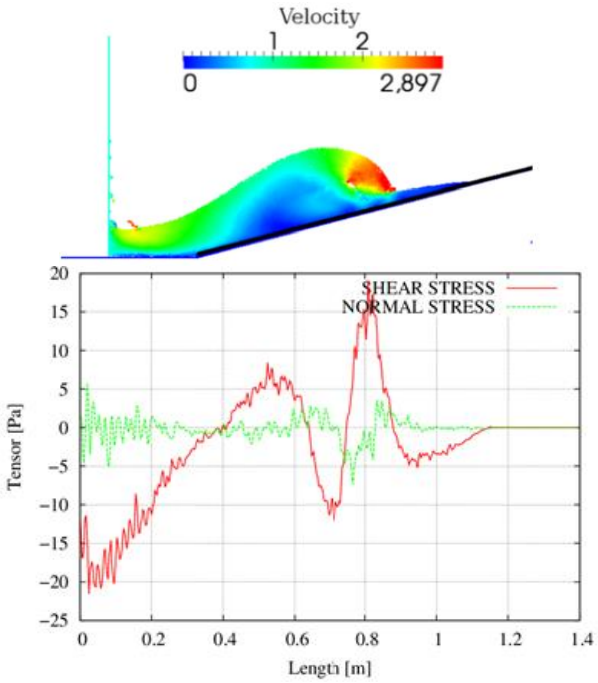

Fig. 11. Velocity field and shear stress on inclined surface (black line) at 15° in 2.14 s.

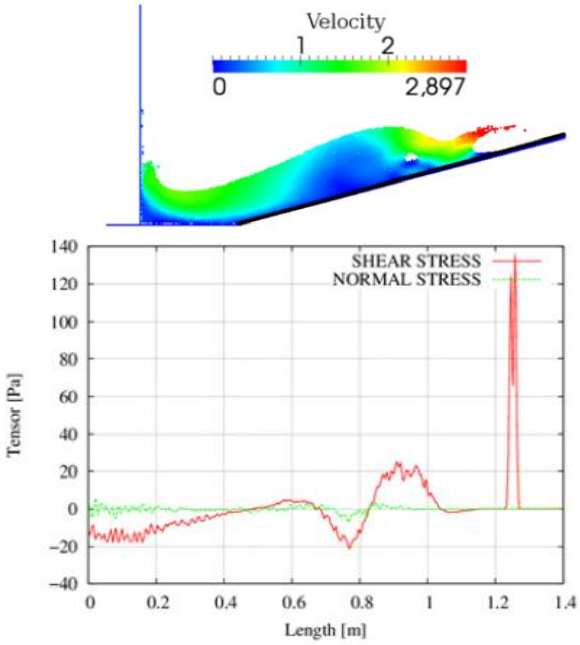

Fig. 12. Velocity field and shear stress on inclined surface (black line) at 15° in 2.23 s.

5. Conclusions

The SPH method was used to study water waves propagation and breaking on inclined surface. The mathematical model considers the compressible continuity equation associated to the incompressible momentum equation, forming the so called weakly compressible smoothed particle hydrodynamics model. Turbulence effect was considered introducing an extra eddy viscosity, calculated by the Smagorinsky SGS model. Several cases involving laminar and turbulent flow were systematically studied in order to identify the correct values for the smoothing length and the XSPH regularizing parameter ε. The benchmark cases are an artificially constructed analytical solution for a cavity, the square cavity shear driven flow, the dam break flow, irregular and single wave propagation, and, finally, the wave impact on inclined surface. Some concluding observations from the investigation are given below.

- Through the constructed analytical solution, it was possible to find that $h = 1.3\Delta x$ and $\varepsilon = 0.3$ leads the XSPH model to correctly recover the flow field for the cavity shear driven flow.
- In the subsequent study of propagating waves, although the best smoothing length have remained unchanged, the XSPH regularizing parameter ε needed to be decreased by one order of magnitude, to prevent the premature damping of the waves, in the dam break flow. We have found that $h = 1.3\Delta x$ and $\varepsilon = 0.03$ always recover very consistent results for the propagating waves simulations performed in the present work, even for the shear stress over an inclined wall.
- In such a way, one conclude that for free surface flows, dominated by inertial waves, the XSPH regularizing parameter must be one order of magnitude small than in viscous flows, despite the smoothing length can be the same.
- The results of the present work allow concluding that SPH code has proved useful to calculate shear stresses. This data are very important for the continuation of this study, which aims at analysing erosion. We were able to analyse the forces exerted by the fluid, but the study on the forces supported by solid particles is still missing.

References

1. Lucy, L.B. (1977). Numerical approach to testing the fission hypothesis. *Astronomical Journal*, 82, 1013-1024
2. Morris, J.P. (2000). Simulating surface tension with smoothed particle hydrodynamics. *International Journal for Numerical Methods in Fluids*, 33(3), 333-353.
3. Liu, G.R.; and Liu, M.B. (2003). Smoothed particle hydrodynamics - A meshfree particle method. *World Scientific*, New Jersey.
4. Hu, X.Y.; and Adams, N.A. (2007). An incompressible multi-phase SPH method. *Journal of Computational Physics*, 227(1), 264-278.
5. Dalrymple, R.A.; and Rogers, B.D. (2006). Numerical modeling of water waves with the SPH method. *Coastal Engineering* 53(2-3), 141-147.

6. Zheng, X.; and Duan, W. (2010). Numerical simulation of dam breaking using smoothed particle hydrodynamics and viscosity behavoir. *Journal of Marine Science and Applications*, 9(1), 34-41.
7. Li, J.; Liu, H.; Gong, K.; Tan, S.K.; and Shao, S. (2012). SPH modeling of solitary wave fissions over uneven bottoms. *Coastal Engineering*, 60, 261-275.
8. Gotoh, H.; Shao, S.; and Memita, T. (2004). SPH-LES model for numerical investigation of wave interaction with partially immersed breakwater. *Coastal Engineering Journal*, 46 (1), 36-63.
9. Violeau, D.; and Issa, R. (2006). Numerical modelling of complex turbulent free-surface flows with the SPH method: an overview. *International Journal for Numerical Methods in Fluids*, 53(2), 277-304.
10. Barreiro, A.; Crespo, A.J.C.; Dominguez, J.M.; and Gomez-Gesteira, M. (2013). Smoothed particle hydrodynamics for coastal engineering problems. *Computer and Structures*, 120, 96-106.
11. Altomare, C.; Crespo, A.J.C.; Rogers, B.D.; Dominguez, J.M.; Gironella, X.; and Gomez-Gesteira, M. (2014). Numerical modeling of armour block sea breakwater with smoothed particle hydrodynamics. *Computer and Structures*, 130, 34-45.
12. Dezbo, E.; Zagar, D.; Krzyk, M.; Cetina, M.; and Petkovsek, G. (2014). Different ways of defining wall shear in the smoothed particle hydrodynamics simulations of a dam-break wave. *Journal of Hydraulic Research*, .52 (4), 453-464.
13. Monaghan, J.J. (2005) Smoothed particle hydrodynamics. *Reports on Progress in Physics*, 1703-1759.
14. Morris, J.P.; Fox, L.P.; and Zhu, Y. (1997). Modeling low Reynolds number incompressible flows using SPH. *Journal of Computational Physics*, 136(1), 214-226.
15. Batchelor, G.K. (1967). An introduction to fluid dynamics. *Cambridge University*, Cambridge.
16. Izza, R. (2004). Numerical assessment of the SPH gridless method for incompressible flows and its extension to turbulent flows. *Ph.D. thesis*. The University of Manchester.
17. Monaghan, J.J. (1992). Smoothed particle hydrodynamics. *Annual Review of Astronomical and Astrophysics*, 30, 543-574.
18. Monaghan, J.J. (1994). Simulating free surface flows with SPH. *Journal of Computational Physics*, 110 (2), 399-406.
19. Crespo, A.A.J.C. (2008). *Application of the smoothed particle hydrodynamics model SPHysics to free-surface hydrodynamics*. Ph.D. thesis. Universidade de Vigo - Departamento de Fisica Aplicada.
20. Donea, J.; and Huerta, A. (2003). Finite Element Method for Flow Problems. *John Wiley and Sons Ltd*, West Sussex, England.
21. Koshizuka, S.; and Oka, Y. (1996). Moving particle semi-implicit method for fragmentation for compressible fluid. *Nuclear Science Engineering*, 123, 421-434.
22. Idelsohn, S.R.; Onate, E.; and Del pin, F. (2004). The particle finite element method: a powerful tool to solve incompressible flows with free-surfaces and

breaking waves. *International Journal for Numerical Methods in Engineering*, 61(7), 964-989.

23. Cox, D.T.; and Ortega, J.A. (2002). Laboratory observations of green water overtopping a fixed deck. *Ocean Engineering*, 29(14), 1827-1840.
24. Gomez-Gesteira, M.; Cerqueira, D.; Crespo, C.; and Dalrymple, R.A. (2005). Green water overtopping analysed with a SPH model. *Ocean Engineering*, 32(2), 223-238.
25. Xiao, H.; and Huang, W. (2010). Effects of turbulence models on numerical simulations of wave breaking and run-up on a mild slope beach. *Journal of Hydrodynamics*, Ser. B, 22(5), 166-171.